

Design of Lawn Care Blade Profiles for Airflow

E.D. Davidge and S.D. Yu

Department of Mechanical and Industrial Engineering,
 University of Ryerson, Toronto, Ontario, Canada M5B 2K37, Canada

Abstract: Computational fluid dynamics models are developed to investigate the airflow induced by cutting blades used in a lawn care cutting pan. The effects of blade profiles on mass flow rates and power consumptions are investigated thoroughly through the computer models. The simulation results are useful for designing the blade profiles that produce desired mass flow rate of air at minimal power. Experiments were carried out to validate the simulation results obtained using the computational models.

Key words: Airflow, blades, computational fluid dynamics, grass cutting

INTRODUCTION

In the lawn care industry, blades are designed to cut grass, draw air into the cutting pan and propel the air and grass clipping mixture into a collector. Some large professional lawn care systems require the usage of an impeller to produce adequate airflow. However, impellers often get clogged with clippings, which may require frequent maintenance. Clogging is highly undesirable because the operator must stop the operation to clean up the clogged location manually. This usually reduces the cutting/collection efficiency considerably. In addition, clogging reduces the collection capacity and often leaves a trail of grass clippings uncollected. This is considered not acceptable, e.g., when cutting grass in a sports field. To eliminate the need of impellers, the modern day blades are often designed to be multifunctional, i.e., grass cutting, clipping impaction and transportation of air-clipping mixtures via a tunnel from the cutting pan to the collector. A typical multifunctional lawn system is shown in Fig. 1.

A review of literature revealed that little was done on the airflow induced by grass-cutting blades. Aside from cutting grass, the blades must be able to produce as much airflow as possible at minimal power consumption. As a result, the cutting blades also act like fan blades. The pressure increase in the air is not as critical as the generated airflow. The blades do not have the same purpose as compressor blades. However, as far as airflow generation is concerned, the cutting blades are similar to fan and compressor blades (Dixon *et al.*, 1998).

A typical professional lawncare system consists of a cutting deck, a transporting tunnel and a collector. The

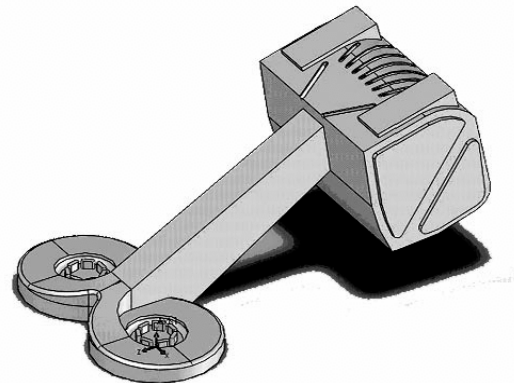


Fig. 1: A twin blade cutting/collection lawn care system

lawn care system is often mounted on a tractor or a zero turn radius vehicle to achieve the desired mobility.

The cutting deck consists of 2 counter-rotational cutting blades and a cutting pan. As the tractor moves along, an area of grass and other vegetation are cut by the 2 rotating and translating blades. At the same time, the high-speed rotational blades create a sufficient flow of air, which is responsible for transporting the clippings and forcing them into a central-rear exit and into the conveying tunnel. A view of the cutting system is shown in Fig. 2. Using the blades for cutting and airflow generation is beneficial because of the elimination of an additional impeller, which is otherwise required for moving the air-clipping mixture.

The conveying tunnel, as part of the lawn care system, transports air-clipping mixtures from the cutting pan to the collector. Clippings exit the cutting system via the rear centre exit path and then enter the tunnel. The

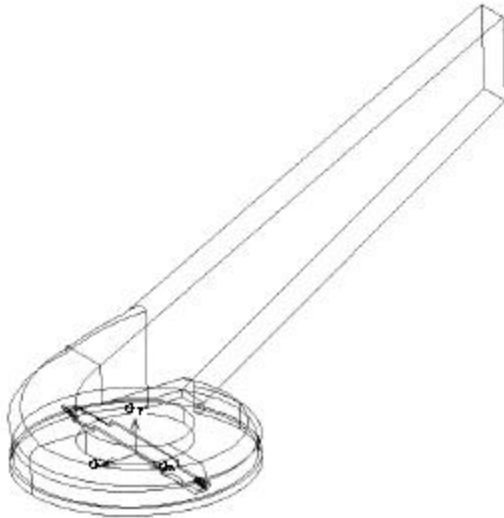


Fig 2: A view of half of a twin-blade cutting system

tunnel is raised at an angle in order to transport the clippings towards the elevated collector.

The collector stores the clippings from the tunnel. The collector is covered in perforated metal vents that allow air to escape while retaining the clippings. A hydraulic-driven mechanism is used to raise the collector and unload the clippings onto a truck for further processing.

The end of a cutting blade is largely responsible for the grass cutting operation and generation of sufficient airflow in the axial and circumferential directions. The airflow in the radial direction is small. For this reason, the system may be modeled as a tube-axial problem due to the low number of vanes (2 only) or vane-axial fan (Kuski, 1997) due to the high nominal linear speed of 96.5 m s^{-1} at the blade tip. Under normal cutting the blades rotate at 269 rad s^{-1} (2569 rpm). The axial and circumferential airflows are determined by the effective 2-D shape of a blade near the end as shown in Fig. 3, for a serrated type of blades and in Fig. 4, for a paddle type of blades. The sharp leading edges of the blades are responsible for cutting grass; the raised trailing edges generate the upward airflow. It is observed in field tests that the serrated blades offer better compaction of clippings; they may not produce the necessary airflow through the system to prevent clogging in harsh conditions. The paddle blades produce sufficient airflow, but consume a great deal of power which can slow the motor down in harsh conditions.

An effective method used to model 2-D axial fans is to transform the endless rotational path of the blades into a finite, linear path as seen in many 2-D axial compressor

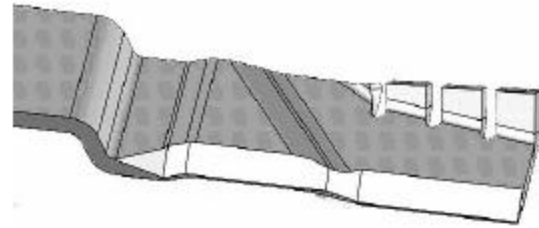


Fig. 3: A detailed view near a serrated-type blade tip

cascade analyses (Doyle, 1971; Saha and Roy, 1997; Farn and Whirlow, 1975; Carstens *et al.*, 2003; Chen *et al.*, 1998; Hilgenfeld *et al.*, 2003). Design of blades by conducting series of three-dimensional analyses is computationally expensive and time consuming. Earlier 3-D studies showed that while 3-D simulations were possible, it was a very lengthy process that would not easily allow many variations in blade shapes. This paper presents numerical simulations of airflows based on 2-D computational dynamics models.

COMPUTATIONAL FLUID DYNAMICS MODELS

Cutting system: The key component in the cutting system is the cutting blades. In this paper, two types of cutting blades of 0.721 m long, shown in Fig. 3 and 4, are studied. For either blade, the cross-section profile varies along the blade length. The tip portion of 8 cm in length plays a critical role in cutting and airflow generation. The inner portion of the blade is not significant in terms of grass cutting and airflow generation. However, as an integral part of the blade, the inner portion is responsible for transmitting power from the hub to the tips. In the 2-D model, the cross section analyzed is taken to be 4 cm from the tip of the blade in order to attain a profile in the middle of the scoop. At this location, the cross section of the blade has a linear speed of 86.5 m s^{-1} .

The transformed linear shape of the cutting pan housing is shown in Fig. 5. GAMBIT, a commercially available software package, is used as a preprocessor for geometry and mesh generation. FLUENT, another commercially available CFD software package, is employed to solve the two-dimensional airflow problem. The linear cutting pan model is 6.1 m long and is capable of simulating airflow for the first three complete turns of the blade. Since, the cutting blade has a cutting edge on each end, the individual blade profiles have a linear spacing of half of the circumference of the rotational blade path. For an effective diameter of 0.641 m, the blade path is 2.014 m. The entire model includes 6 blade profiles and three tunnel outlets. The outlets are raised by 32° to represent a tunnel of 35 cm in length and 18 cm in height.

The actual tunnel is 1.6 m long and connects the cutting pan to the collector where the clippings are stored. In this model, the actual tunnel and collector are not included because the focus is on the blade profile design and normalized power consumption. The height of the horizontal cutting pan area used is 11 cm. This height may vary as the cutting height on the actual lawn care system is adjustable.

It is necessary to include several blade configurations in a computational model because the airflow needs certain distance to develop as it passes from one blade to the next. Usually six to ten configurations are sufficient for the flow to be fully developed in a 2-D compressor cascade (Wallis, 1983). The 2-D model shown in Fig 5 has a blade spacing of 1.007 m and a blade length of 0.065 m. The length ratio is about 15. The interference effects from one blade to another can be considered negligible when the blade spacing to length ratio is greater than or equal to three in conventional axial-bladed systems (Dixon, 1998). In many axial flow systems, the top edge is open so that the air can flow directly through. However, the lawnmower system has a wall on the top edge, which prevents the passage of air. The closeness of a wall to the blades may induce more severe interference effects. As a result, six blade configurations were used in the model.

In all cases studied in this research, the blades are positioned such that the leading edge of every other blade coincides with the midpoint of a tunnel outlet. It is understood that the instantaneous steady-state flow field surrounding the blades will vary as they move through the cutting pan; however, this position was chosen as the common position in which all the blade profiles will be analyzed. Since, the actual blades have 2 scoop profiles

per blade, results obtained in a 2-D model must use the combined effect of two adjacent blade profiles.

Boundary conditions: In all computational models, the inlet and outlet surfaces are set to have zero gauge pressure because these surfaces are exposed to the atmosphere. The velocity through the edge nodes may change. However, it will not affect the zero gauge pressure. Since, the inlet and outlet surface pressures are equal, there is no back-pressure load on the system after it has been solved for steady-state. In real tests, the pressures at the inlet and outlet deviate slightly from atmospheric conditions, but it is difficult to apply a specific pressure at the 2-D edges since they cannot be found directly from test rig measurement.

A test was conducted to see whether the gap between the bottom of the blade and the inlet surface provided enough computational space to allow the pressure to deviate from atmospheric conditions. Two cases were examined and are shown in Fig 6. The first case has a gap of 1 cm between all the blades and the inlet, the second case has a gap of 15 cm. The results are tabulated in Table 1.

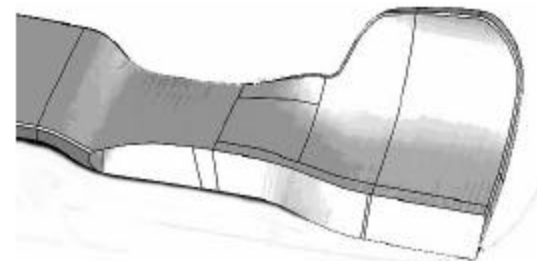


Fig. 4: A detailed view near a paddle-type blade tip

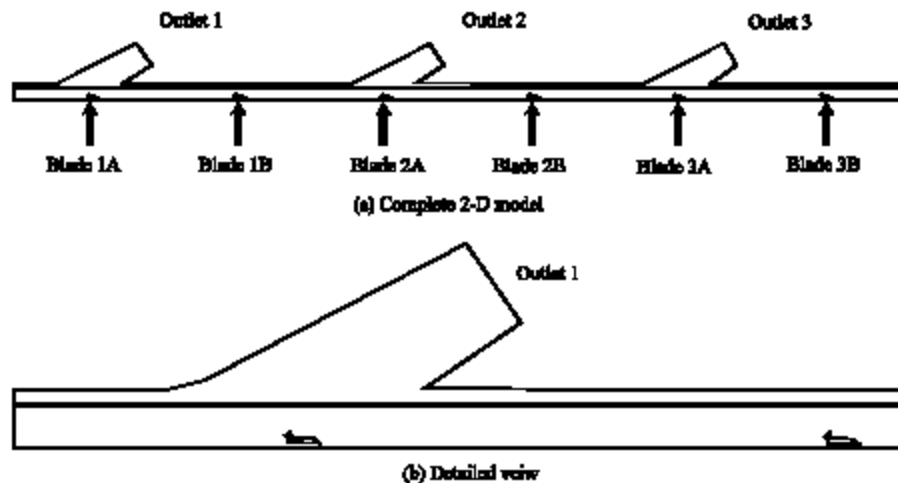


Fig. 5: Linearly transformed cutting pan housing

Table 1: Effect of inlet gaps on airflow

Gaps (cm)	Drag force (N)	Mass flow rate (kg s ⁻¹)
1	180	6.99
15	158	6.97

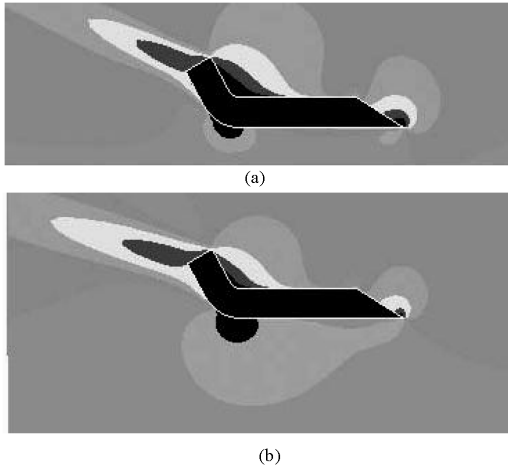


Fig. 6: Total pressure contours around blade with inlet gaps of (a) 1 cm (b) 15 cm

The mass flow rates for the two cases are the same. The drag force acting on the blades for the 1 cm gap case is larger than that for the 15 cm gap case. The pressure regions surrounding the blade are the same in both cases. The extra computational domain with the 15 cm gap allows for a smaller pressure gradient under the blade; however, much of extra space is not needed and only adds to the size of the model. In this study, the lower 1 cm gap is used in optimal blade designs.

To complete the boundary conditions, the bottom zone was set as the MRF with a translational velocity of 86.5 m s⁻¹ to the right. All blade surfaces have their adjacent cell zones as the MRF; therefore, in momentum options, the blade walls are defined as moving walls relative to adjacent cell zone at a translational speed of 0 m s⁻¹ to the right.

Grid analysis: Meshing begins on the edges of each blade with a spacing of 1 mm. A boundary layer mesh was created with 4 rows. The first row is 0.5 mm from the surface and uses a growth rate of 1.2. The MRF area and upper area were meshed with a Tri-Pave scheme with a 5 mm interval size as shown in Fig. 7. The same technique was used to create 2 other meshes described in Table 2. The numerical results for the drag forces and the mass flow rates, obtained using the 3 different meshes, are given in Table 3. It can be seen that the three meshes yield consistent results. Consequently, the medium sized

Table 2: Grid analysis parameters

Mesh parameters	Meshes		
	Coarse	Medium	Fine
Edge interval (mm)	2.0	1.0	0.5
First row height (mm)	1.0	0.5	0.25
Tri-pave interval size (mm)	10.0	5.0	2.5
Number of elements	32,263	125,910	478,724

Table 3: Drag force and mass flow rate computed using difference mesh schemes

	Meshes		
	Coarse	Medium	Fine
Drag force (N)	7.13	7.22	7.27
Mass flow rate (kg s ⁻¹)	0.558	0.562	0.550

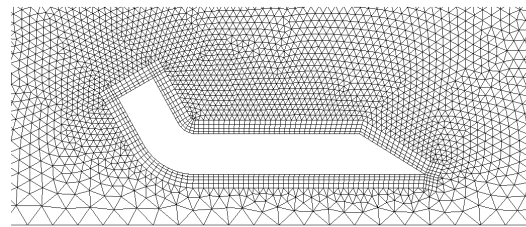


Fig. 7: Medium mesh around blade profile
























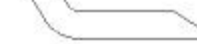
mesh parameters were used in all studies to achieve a balance of computational time and accuracy.

Solution parameters: The solver is set-up as 2-D, time-steady, segregated and implicit. The energy equation is not used in the system as temperature rise is not a concern. A standard k-ε turbulence viscous model is used with default constant values of C_μ = 0.09, C_{1ε} = 1.44, C_{2ε} = 1.92, σ_ε = 1.3, σ_κ = 1.0. These values were determined from experiments with air and water and have been found to work well for wall-bounded flows (Fluent, 2003). The properties of air are constant density of 1.225 kg m⁻³ and constant viscosity of 1.789E-05 kg ms⁻¹. The operating pressure is 101.325 kPa. The gravity was set to -9.8 m s⁻², down. The no-slip condition is used.

Blade profiles: A total of 23 blade profiles were studied. The 2 blade shapes, shown in Fig. 8, used in the industry, are chosen as the reference blade profiles. The chord lengths of the profiles are 6.2 and 9.5 cm, respectively. Each profile is 8 mm thick and has a 30° cutting edge.

New blade profiles may be created based on the first reference profile, which has a 1.6 cm tail raised at 60°, located 3.2 cm behind the cutting edge. The features of the tail that were altered are the tail length, tail angle and the tail position with respect to the cutting edge. The features that are kept constant in all profiles are the 8 mm thickness and 30° cutting edge. The original tail length of

Table 4: Different profiles obtained from the serrated blade

Eight Blade Profiles of Varying Tail Lengths	Eight Blade Profiles of Varying Tail Angles	Eight Blade Profiles of Varying Tail Positions
 0.6 cm	 15°	 0.7 cm
 1.1 cm	 30°	 1.2 cm
 1.6 cm	 45°	 1.7 cm
 2.1 cm	 60°	 2.2 cm
 2.6 cm	 75°	 2.7 cm
 3.1 cm	 90°	 3.2 cm
 3.6 cm	 105°	 3.7 cm
 4.1 cm	 120°	 4.2 cm

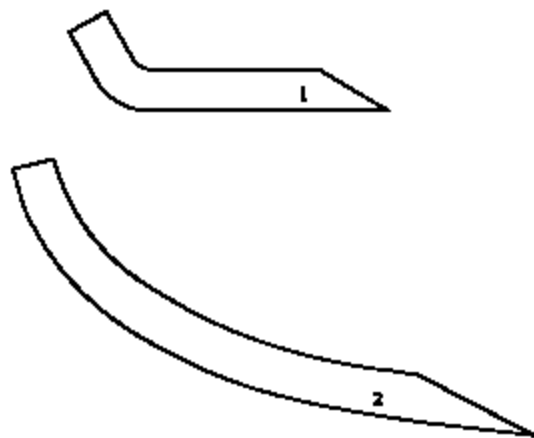


Fig. 8: Two actual profiles for the serrated and paddle types of blades

the first reference profile is 1.6 cm and is varied from 0.6-4.1 cm, in 0.5 cm increments. The profiles by varying the tail lengths are shown in Table 4. The original tail angle of the first profile 1 is 60° and is varied from 15° to 120°, in 15° increments to obtain the second group of blade profiles in Table 4. The first reference profile has the raised tail near the back. Typical efficient aerofoil shapes have camber lines that are either circular or parabolic from

front to back (Wallis, 1983). The tail position is varied, while keeping the length of the tail the same as in the first reference profile. These profiles, shown in Table 4, represent blades created using stock material of varying width. The original tail position of the first reference profile is 3.2 cm behind the cutting edge. The position is varied from 0.7 -4.2 cm, in 0.5 cm increments.

NUMERICAL RESULTS

The initial model exhibited some numerical instability when the velocity boundary condition was applied directly to the blades. This was most likely caused by the high degree coupling between the 2 momentum equations when the influence of a rotational or translational term is large (Fluent, 2003). The Multiple Reference Frame (MRF) can be used to remedy this problem. The MRF creates a local reference frame that has the same velocity as the moving components, or zero velocity relative to the moving blades. In an analysis, there are two reference frames-one moving and one stationary. Use of the MRF enhances the numerical stability so that convergence can be achieved. It is noted that the MRF is approximate and only works for steady-state flows. However, it provides a reasonable model of the time-averaged flow for an application (Fluent, 2003). The MRF zone must be a

Table 5: Numerical results of the two reference blade profiles

Reference profiles	Mass flow rate (kg s ⁻¹)	Power (kW)	Efficiency ratio (kg/s/kW)
1	0.56	1.25	0.45
2	0.71	2.46	0.29

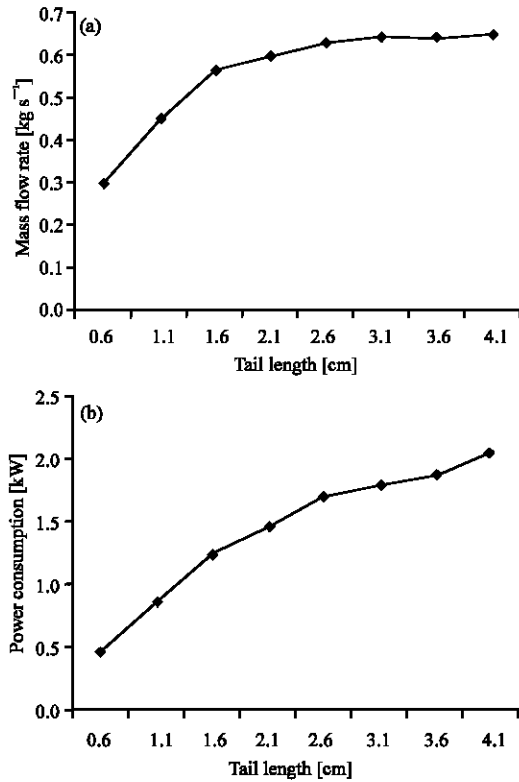


Fig. 9: Effects of tail lengths on (a) mass flow rate of various and (b) power consumption

straight rectangular shape for a translational path. In the final model, the MRF zone begins 2.5 cm below the top of the cutting pan ceiling and goes to the base inlet surface.

The computed quantities include the mass flow rate at outlet 3 and the drag force on blades 2B and 3A. The power consumption was determined by multiplying the drag force by the arm of 0.321 cm. The blades spin at 269 rad s⁻¹ (2570 rpm). The original results outputted were per meter depth into the third dimension; the results presented in this study have been adjusted for an 8 cm depth. The efficiency ratio used in the results is a ratio of mass flow rate to power consumption. The higher the ratio, the better the performance of the blade profile. The mass flow rates and the power consumptions along with the efficiencies for the 2 reference profiles are given in Table 5.

Effects of tail lengths: Eight computational models were developed to study the effects of the blade tail lengths.

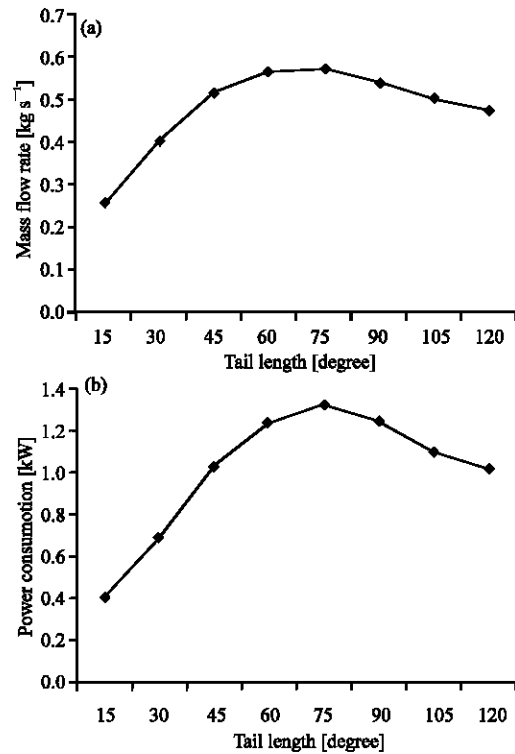


Fig. 10: Effects of tail angles on (a) mass flow rates and (b) power consumption

The computed mass flow rates and power consumptions versus the tail lengths are shown in Fig. 9. It can be seen that the mass flow rates plateau with a tail length of 2.6 cm even though the power consumption continues to increase. This demonstrates that first group of profiles can only generate a limited amount of air flow. The more efficient profiles are those having the shorter tail lengths. The efficiency, defined as the ratio of the mass flow rate per unit power consumption, decreases consistently with the increasing tail length.

Effects of tail angles: Simulation results for the second group of blade profiles are shown in Fig. 10. The mass flow rate reaches a maximum at a tail angle of 75°. The maximum power consumption occurs with a tail angle of 75°. The lowest efficiency ratio also occurs at 75°. This demonstrates that the efficiency ratio is derived more from the correlation of increasing power consumption with increasing mass flow rate and less from the similarity of the angle of the resulting velocity vector (sum of horizontal blade velocity and relative blade outlet flow velocity) to the tunnel angle. The highest efficiency ratios occur with the lowest tail angles. This can be attributed to the lesser amount of turbulence created by the low angles compared to the high angles. The large angles induce

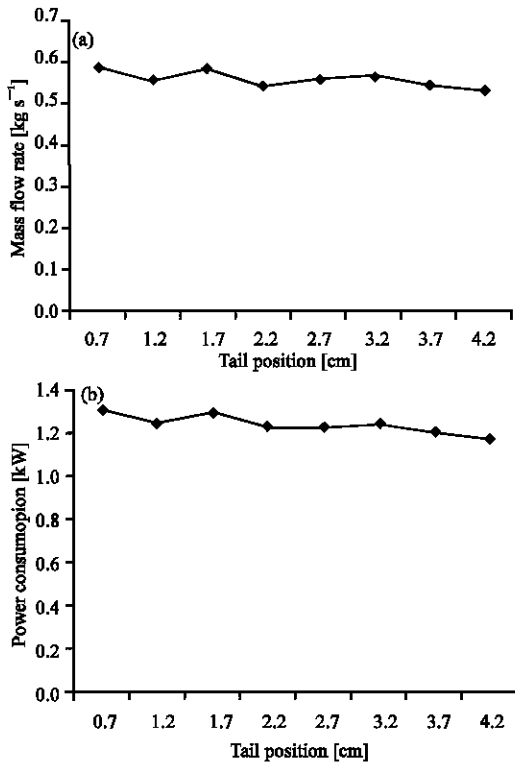


Fig. 11: Effects of tail positions on (a) mass flow rate of various and (b) power consumption

more flow separation behind the tail, which leads to turbulence and wasted energy. This phenomenon was observed in the outputted turbulence contours.

Effects of tail positions: The simulation results obtained by varying the tail positions are shown in Fig. 11. The mass flow rate and power consumption are not significantly influenced by the tail positions. The efficiency for various tail positions remains the same.

RESULTS

Experiments were conducted mainly to validate the computer models. The experimental studies were performed using a test rig shown in Fig. 12. The test rig consists of a complete cutting system. The rig includes one cutting pan with liner, 2 sets of blades, one conveying tunnel, one collector, one hydraulic drive motor and a 10-hp electric motor. The dimensions of the cutting pan are 141 cm (54 in) by 82 cm. The tunnel is 128 cm long and has interior width of 24 cm. The height of the tunnel interior varies along the length of the tunnel, from 35 cm at the base to 28 cm at the top. The test rig is

modular and allows testing of the system with and without the collector. In order to achieve the desired blade tip linear speed of 19,000 fpm at 2,569 rpm, a belt with a required pulley ratio was added between the electric motor and the blades.

The test rig was set up with the tunnel fully raised (30°) and with a 2.54 cm gap between the ground and the bottom of the cutting pan. Early test rig experiments did not have the collector attached in order to concentrate on the cutting pan and tunnel. The first computational models did not incorporate the collector. Testing of airflow with the collector integrated is done in the later experimental and computational models. The serrated type of blades was used in the experiments.

The base of the cutting pan and blades are raised 1.37 m off the ground. The cutting pan is fixed to the support frame. The air inlet gap at the bottom of the pan is adjusted by moving a clear plastic sheet up and down in relation to the fixed cutting pan. This simulates the gap between the ground and the cutting pan in the lawn-care tractor. The tunnel is held in place by straps fastened to the frame. The inclination angle of the tunnel can be adjusted easily by tightening the straps.

In order to take readings inside the tunnel, holes were drilled in the plastic cover. The holes were drilled in a line that is perpendicular to the airflow so that a cross-section grid of airflow measurements could be taken. The holes were covered with duct tape when not in use so as to not disrupt the airflow. Measurements were not taken from inside the cutting pan for several reasons. The main reason is that the probe must be protected from any damage. Another reason is that a large amount of turbulence was expected within the cutting pan and readings may be unreliable because the Pitot tube sensor used does not accurately measure heavily turbulent flows (White, 1999). Readings were taken from the base of the tunnel where the air exits the cutting pan and the end of the tunnel. Six readings were taken, 3 from an area near the blades at the base of the tunnel and three from the end of the outlet. The readings at each location were taken in a vertical path in the centre of the tunnel. There was a high reading (5 cm from the top of the tunnel), a medium reading (17.8 cm from the top of the tunnel) and a low reading (28 cm from the top of the tunnel). Figure 13 shows how the Pitot tube sensor is positioned through the hole and its orientation with respect to the tunnel. The results of the velocity measurements are compared with the simulation results in Table 6. The errors between the experimental velocities and the computed velocities are reasonably small.

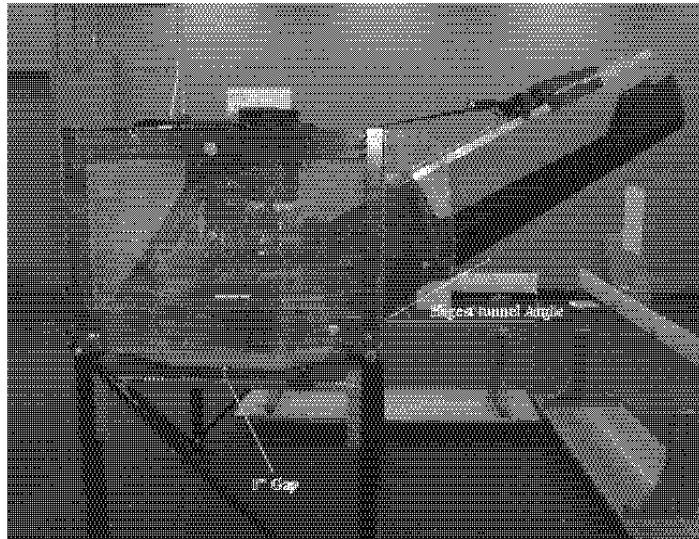


Fig. 12: Test rig setup without a collector

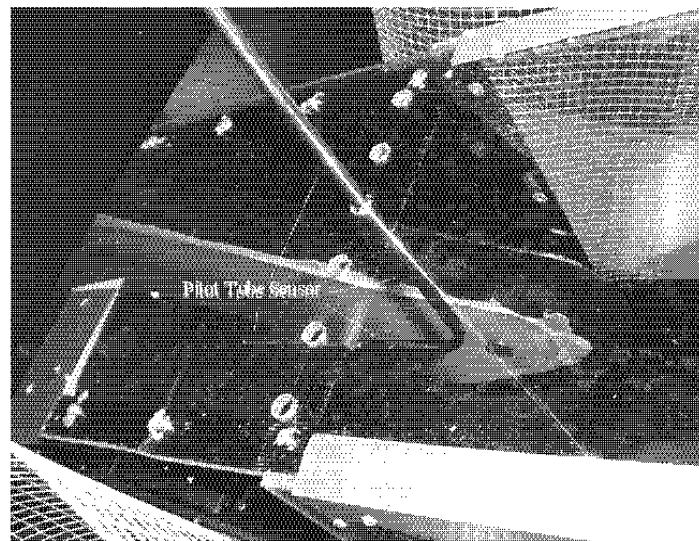


Fig. 13: Pitot tube inserted into tunnel

Table 6: Comparisons between simulations and experiments for the serrated blades

Distance from top of tunnel, cm (inch)	Experimental velocities ($m s^{-1}$)	Computed velocities ($m s^{-1}$)	Error (%)
5.0 (2)	18	15	-18.9
17.8 (7)	15	13	-13.3
28.0 (11)	14	12.5	-10.7

CONCLUSION

Effects of lawn care blade shapes on the mass flow and power consumption were studied using two dimensional computational dynamics models in this study. The results presented in this study are new and applicable to blade design in the lawn care industry.

REFERENCES

- Carstens, V., R. Kemme and S. Schmitt, 2003. Coupled simulation of flow-structure interaction in turbomachinery. *Aerospace Sci. Tech.*, 7: 298-306.
- Chen, W.L., F.S. Lien and M.A. Leschziner, 1998. Computation prediction of flow around highly loaded compressor cascade blades with non-linear eddy viscosity models. *Int. J. Heat Fluid Flow*, 19: 307-319.
- Dixon, S.L., 1998. *Fluid Mechanics and Thermodynamics of Turbomachinery*. 4th Edn. Butterworth-Heinemann, Boston, USA.

- Doyle, M.D.C., 1971. Advanced through-flow analysis applied to a low-speed axial flow compressor. *Int. J. Mech. Sci.*, 13: 833-842.
- Farn, C.L.S. and D.K. Whirlow, 1975. Design estimate of cascade performance. *Computers and Fluids*, 3: 225-233.
- Fluent User's Manual, 2003. Fluent Inc.
- Hilgenfeld, L., P. Cardamone and L. Fottner, 2003. Boundary layer investigations on a highly loaded transonic compressor cascade with shock/laminar boundary layer interactions. *Proc. Inst. Mechanical Eng.*, 217 (4): 349-356.
- Kuski, T.D., 1997. Understanding Axial Fans. *Plant Eng.*, 51 (2): 96-98.
- Lewis, R.I., 1996. *Turbomachinery Performance Analysis*. John Wiley and Sons, Toronto, Canada.
- Saha, U.K. and B. Roy, 1997. Experimental investigations on tandem compressor cascade performance at low speeds. *Exp. Thermal and Fluid Sci.*, 14: 263-276.
- Wallis, R. Allan, 1983. *Axial Flow Fans and Ducts*. John Wiley and Sons, Toronto, Canada.
- White, F.M., 1999. *Fluid Mechanics*. 4th Edn. McGraw-Hill, Toronto, Canada.